World Academy of Science, Engineering and Technology
International Journal of Bioengineering and Life Sciences
Vol:8, No:9, 2014

Bio-Heat Transfer in Various Transcutaneous Stimulation Models

Trevor E. Davis, Isaac Cassar, Yi-Kai Lo, Wentai Liu

***Abstract*—**This study models the use of transcutaneous electrical nerve stimulation on skin with a disk electrode in order to simulate tissue damage. The current density distribution above a disk electrode is known to be a dynamic and non-uniform quantity that is intensified at the edges of the disk. The non-uniformity is subject to change through using various electrode geometries or stimulation methods. One of these methods known as edge-retarded stimulation has shown to reduce this edge enhancement. Though progress has been made in modeling the behavior of a disk electrode, little has been done to test the validity of these models in simulating the actual heat transfer from the electrode. This simulation uses finite element software to couple the injection of current from a disk electrode to heat transfer described by the Pennesbioheat transfer equation. An example application of this model is studying an experimental form of stimulation, known as edge-retarded stimulation. The edge-retarded stimulation method will reduce the current density at the edges of the electrode. It is hypothesized that reducing the current density edge enhancement effect will, in turn, reduce temperature change and tissue damage at the edges of these electrodes. This study tests this hypothesis as a demonstration of the capabilities of this model. The edge-retarded stimulation proved to be safer after this simulation. It is shown that temperature change and the fraction of tissue necrosis is much greater in the square wave stimulation. These results bring implications for changes of procedures in transcutaneous electrical nerve stimulation and transcutaneous spinal cord stimulation as well.

***Keywords*—**Bioheat transfer, Electrode, Neuroprosthetics, TENS, Transcutaneous stimulation.

I. Introduction

TRANSCUTANEOUS Electrical Nerve Stimulation (TENS) is a non-invasive form of electrotherapy that aims to treat neuropathic and musculoskeletal pain [1]-[3]. TENS functions through transcutaneously stimulating sensory nerves in order to treat pain. TENS therapy is an FDA approved method of treating pain, yet it can involve stimulation that breaches the threshold of a patients pain. An additional therapy that follows the same principles as TENS is transcutaneous spinal cord stimulation (TSCS). TSCS involves transcutaneously stimulating the spinal cord in order to re-enable paraplegic patients to stand or walk again [4], [5]. Parameters for TSCS are more intense than TENS stimulation and involve a disk electrode as the current injection source with proper positioning of a counter electrode. Both of these therapies are being used as treatment methods in medicine and in the research field, yet in order to determine the effectiveness of these therapies, a model of the system is necessary. So far, the models in this field have to do with replicating the dynamic current density distributions of disk electrodes and less focus is placed on the bio-heat transfer. The bio-heat transfer process can show just how much temperature change and tissue damage is inflicted on the site of interest. This study aims to model the general bioheat transfer process before more intensive and realistic stimulation parameters are considered.

The injection parameters of standard TENS systems for treating pain can vary greatly. One of the more extreme methods is Brief Intense TENS, which is used to treat strong pain through stimulating the nervous system with high intensity current. However, it can sometimes be too strong of stimulation for patients to endure [1]-[3]. This simulation looks at an example method of reducing tissue injury which can later be adopted and modified for the parameters of Brief Intense TENS or TSCS, which is even more severe than TENS stimulation [4], [5] in order to address methods of reducing the severity of possible tissue damage. There is a great need for an accurate model of the TENS and TSCS systems and this model addresses the initial necessary step of modeling the bioheat transfer process due to electromagnetic heating before these other computationally demanding studies are done.Further research will involve a more powerful computation tool that can accurately model these parameters.

In all of these therapies, the stimulation tool is some derivative of a disk electrode. The behavior of disk electrodes has been well characterized for quite some time, and is still being studied [6]-[9]. Newman determined that the electric field and, by virtue of proportionality, the current density of a disk electrode are intensified at the edges of a disk electrode [10]. This phenomenon was then shown to be dynamic as the double layer capacitance of electrodes was more adequately described first by Helmholtz, and later by Stern, Gouy and Chapman [10]-[12]. They found that the electric double layer of an electrode will redistribute the spatially varied current density to be more uniform over the electrode. A greater current density, as it pertains to stimulating biological mediums, may result in tissue damage [13]-[15]. Through advanced modeling, various electrode geometries and stimulation parameters have been designed in order to reduce this phenomenon [16].

In this study, one of these stimulation designs, termed edge-retarded stimulation [13], is further explored to demonstrate the applications of novel stimulation designs in

Trevor Davis is an undergraduate bioengineer at UCLA, Los Angeles, CA 90095 USA (phone: 858-449-7669; email: sdtrevordavis@gmail.com).

Isaac Cassar is an undergraduate bioengineer at UCLA, Los Angeles, CA 90095 USA (phone: 831-319-8483; e-mail: icazzar@gmail.com).

Yi-Kai Lo and Wentai Liu are with the University of California, Los Angeles, CA 90095, USA (e-mail: yikai.lo@ucla.edu,wentai@ucla.edu).

The project is partially supported by grants from California Capital Equity LLC, UC Laboratory Research Fee Program, and NSF ERC BMES.

bioheattransfer. It has been shown to decrease the effects of intensified current densities at the edges of disk electrodesand hypothetically, a decreased current density will reduce the tissue damage at the edge of a disk electrode. This study tests that hypothesis through comparing the damage and temperature changes induced by edge-retarded stimulation to a standard square wave and serves as the first step of many in the realm of modeling neuroprosthetics and bioheat transfer.

II. Materials and Methods

A. Model Overview

In order to determine how the electrodes in TENS will interact with the tissue during stimulation, models were created using the partial differential equation solver COMSOL Multiphysics ver. 4.4 (COMSOL, Burlington, MA). The models took into account the current stimulation parameters, the electrode interactions with tissue, and the bioheat created as a result of these interactions. COMSOL solves the models through implementing the various constraints to the system and calculating a solution with the finite element method. To simulate the effects of this current injection electrode in the tissue, the Electric Currents interface of the AC/DC module and Bioheat interface of the Heat Transfer module were used and will be discussed in detail later on.

B. Geometry

The disk electrode is constructed in cylindrical coordinates as a two dimensional axisymmetric cross-section (Fig. 1). The axis of symmetry lies on the left axis of the model and rotation about this axis allows for a three dimensional visualization of the model. The electrode is modeled as a platinum disk of radius *a* sitting beneath a layer of tissue which is 10*a* thick and 6*a* wide, while the area to the right of the electrode in Fig. 1 is represented as air.

For this multi-physics coupled problem, many material properties were needed to simulate an accurate model of a disk electrode on human tissue. The multi-layered nature of the biological tissue was represented as one lumped sum of material properties. For the sake of this initial characterization model, this is a safe assumption to describe a general reaction to stimulation. Properties needed to model bioheattransfer, such as the thermal conductivity, specific heat capacity, and density, were found in [17]. The conductivity, σ, and other dielectric properties needed to model current traveling through the human tissue were acquired through other works written on the matter [18]-[20].

As previously stated, the disk electrode has been well characterized [6]-[14]. The theoretical resistance of a semi-infinite medium with conductivity σ above a disk electrode of radius *a* [8] is known as

$$R_s = \frac{1}{4\pi a\sigma}. \quad (1)$$

The double layer capacitance that forms above the electrode with capacitance per unit area γ [11]-[12] is known as

$$C_{dl} = \gamma\pi a^2 . \quad (2)$$

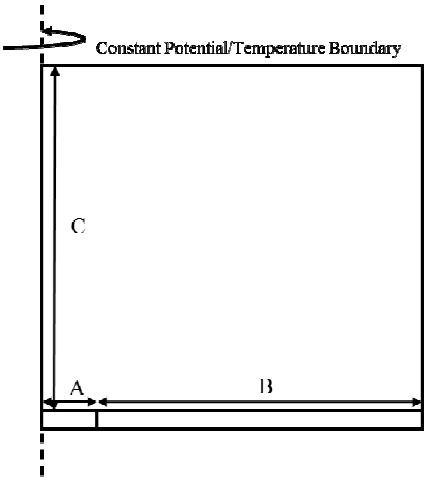

Fig. 1 Thisis a schematic of the electrode-tissue system. The dotted line is the axis of symmetry and the geometry is calculated through rotational symmetry about this axis to simulate a three dimensional system. The electrode (A) has a radius *a*, the air domain (B) extends outwards a distance of *5a* and is the same height as the electrode. Lastly, the tissue domain (C) extends upwards *10a* and outwards *6a*. The top boundary of the tissue is where the constant potential and constant temperature boundary condition is implemented

The time constant that characterizes this electrode, modeled as an RC circuit [11], is then

$$\tau = R_s C_{dl} . \quad (3)$$

The resistance above this electrode follows the example of previous work done to characterize a disk electrode in COMSOL [13], [14]. Due to the finite constraints of a simulation the resistance is separated into a distributed component and a lumped component. The tissue creates resistance based on its conductivity to model the distributed resistance from the electrode up to the potential implemented on the top boundary of the tissue. This boundary potential is calculated through multiplying the current at that boundary by the lumped resistance

$$R_{lumped} = \frac{1}{2\pi\sigma}\left(\frac{1}{r_{min}} - \frac{1}{r_{max}}\right) = \frac{1}{20\pi\sigma a} \quad (4)$$

$$r_{min} = \sqrt{(10a)^2 + r^2}\Big|_{-5a}^{5a} \quad (5)$$

$$r_{max} = \infty. \quad (6)$$

C. Mesh Design

The mesh used to solve this finite element model was constrained to a size of a/50 on the disk edge and a/5 on the tissue-air interface edge. This mesh design also used a growth factor of 1.2 which constrained the next tetrahedral in the mesh from being greater than the previous mesh element by this factor. This meshing was checked through adaptive mesh refinement to ensure that large gradients within the model were not overlooked and misrepresented. This mesh design was used in order to reduce the computational requirements of this lengthy model.

D.Electrical Boundary Conditions

The boundary conditions and initial conditions for this model follow those outlined in [13] and [14].Following is a summary of the equations solved for and boundary conditions implemented.

Laplace's equation was solved in the resistive medium

$$\nabla \cdot J(r,z,t) = 0 \tag{7}$$

$$E(r,z,t) = -\nabla\phi(r,z,t) \tag{8}$$

$$J(r,z,t) = \sigma E(r,z,t) + \frac{\delta D(r,z,t)}{\delta t} \tag{9}$$

as J is the current density, E is the electric field, ϕ is the electric potential and D is the displacement electric field. The boundary potential Dirichlet condition was derived through

$$I(t) = \int (\hat{n} \cdot J(r,z,t)|_{z=10a})\, dr \tag{10}$$

$$V_{bound} = I(t)R_{lumped}. \tag{11}$$

A constant current density

$$J_{stim} = \frac{100mA}{\pi a^2} \tag{12}$$

was applied at the base of the electrode simulating current driven stimulus. This current density interacted with capacitance imposed on the electrode surface to cause the dynamic, non-uniform current density that has been so well studied in the past [6], [7], [10], [13], represented by

$$\hat{n} \cdot J(r,t) = \sigma\nabla\phi(r,t)|_{z=0} + \gamma\frac{\delta}{\delta t}(\nabla\phi(r,t)|_{z=0}). \tag{13}$$

At time $t = 0$, there should be no electric potential in any domain because there have not been any pulses on the electrode yet. Shaping the stimulation pulses to have no current at time zero allows for well-matched initial conditions in the model that will yield a higher likelihood for convergence and represent real-life conditions. Lastly, the tissue and air is modeled to be electrically insulating, meaning no current density enters or leaves the model except through the source of the electrode and the sink of the top boundary of the tissue.

E. Bioheat Transfer Boundary Conditions

The Bioheat Transfer module used to demonstrate the effects of electromagnetic heat transfer on to tissue uses the bioheat transfer equation derived by Pennes [17]. This equation states

$$\rho C\frac{\delta T}{\delta t} = \nabla(k\nabla T) - \rho_b\omega_b C_b(T - T_b) + Q_{met} \tag{14}$$

where ρ, C, k are the density, specific heat and thermal conductivity of the tissue, respectively, ρ_b, ω_b, C_b are the density, perfusion rate and specific heat of the blood, respectively, and T, T_b, Q_{met} are the tissue temperature, arterial blood temperature and metabolic heat rate of the tissue, respectively. The values of these material constants as well as electromagnetic constants of the tissue are shown in Table I. The electrode and the air are assumed to initially be at equilibrium with the standard skin temperature of 34^0C while the skin is represented with an initial temperature of 37^0C.

TABLE I
VARIABLES USED IN MODEL

Variable	Value	Definition	Source
ε	29010	Permittivity of skin	[18]-[20]
σ	0.03 [S/m]	Conductivity of tissue	[18]-[20]
ρ	1200 [kg/m^3]	Density of tissue	[17]
C	3300 [J/(kg·K)]	Specific heat of tissue	[17]
ω	0.00125 [s^{-1}]	Blood perfusion rate of tissue	[17]
k	0.45 [W/(m·K)]	Thermal conductivity of tissue	[17]
ρ_{blood}	937 [kg/m^3]	Density of blood	[17]
C_{blood}	3889 [J/(kg·K)]	Specific heat of blood	[17]
K_{blood}	0.64 [W/(m·K)]	Thermal conductivity of blood	[17]
Q_{met}	0.0 [W/m^3]	Metabolic rate of tissue	[17]
ε_{em}	0.98	Surface emissivity of skin	[17]
E	0.627 [MJ/mol]	Activation energy of tissue	[21]-[22]
A	3.1E98 [s^{-1}]	Frequency factor of tissue	[21]-[22]

Table I provides a thorough list of the material constants of the selected tissue being studied. The permittivity of conductivity of tissue was found through the conductivity of wet tissue with electrode gel on it.

The boundary conditions of this model began at the domain level and proceeded to edge specific conditions. The electrode domain was selected to be a heat source equal to the total power dissipated from the electrode described with

$$Q(r,z,t) = J(r,z,t) \cdot E(r,z,t). \tag{15}$$

This describes resistive or ohmic heating due to electric current. Within the boundaries of the model the surface of the electrode was described as the source of the resistive heating into the tissue. The top boundary of tissue was marked with a Dirichlet condition maintaining constant body temperature at 37^0C to make it a sink of temperature and energy. The layer of skin exposed to the air was allowed to dissipate heat through ambient cooling described by

$$-n \cdot (-k\nabla T) = \epsilon\sigma(T_{amb}^4 - T^4) \tag{16}$$

whereT_{amb} is the ambient skin temperature of 34^0C. The boundary of air at the bottom edge of the geometry was allowed to be open, which simulates the open flow of heat fluxes in and out of the system. This condition assumes that heat flows in and out at ambient skin temperature.

Lastly, the tissue was simulated with the ability to undergo damage. The tissue damage was described through the Arrhenius equation written as

$$\alpha = \int_0^t Ae^{-\frac{E}{RT}} \tag{17}$$

whereα is the degree of tissue damage, A is the frequency factor, E is the activation energy, R is the gas constant and T is the temperature [21], [22]. This integral calculates the energy accumulated in the tissue over time; however, this quantity, α, is difficult to visualize and tissue damage is better represented through

$$\theta_d = 1 - e^{-\alpha}. \tag{18}$$

Equation (18) represents the fraction of tissue necrosis. A value of .349 corresponds to first degree burns, .632 corresponds to second degree burns and a value of 1 corresponds to third degree burns with complete and total cell death [22]. These values areplotted in the results giving a quantifiable representation of how much tissue has been damaged.

F. Stimulation

This model uses two separate stimulation parameters in order to compare their effects on tissue damage. The parameters tested are chosen to illustrate what can be simulated with this bioheat model. They only serve as an example and not realistic parameters used in medicine. The first is normal square wave (Fig. 2A) current injection with a 60mA current pulsed in biphasic stimulation with a 200ms pulse width and a frequency of 80Hz for each pulse, equating to 12.5ms between each 200ms pulse. The second parameter is the previously described edge-retarded stimulation (Fig. 2B) [4], [5]. The edge-retarded simulation ramps up to the desired current intensity of 60mA in one time constant τ and switches to the opposite phase in two time constants. The duration of the pulse was modified to equal the same of amount of charge per pulse as the standard square wave. This experimental parameter is chosen to demonstrate the biological consequences of using stimulation methods that favor reduced current density distributions. Both waveforms are shown in Fig. 2.

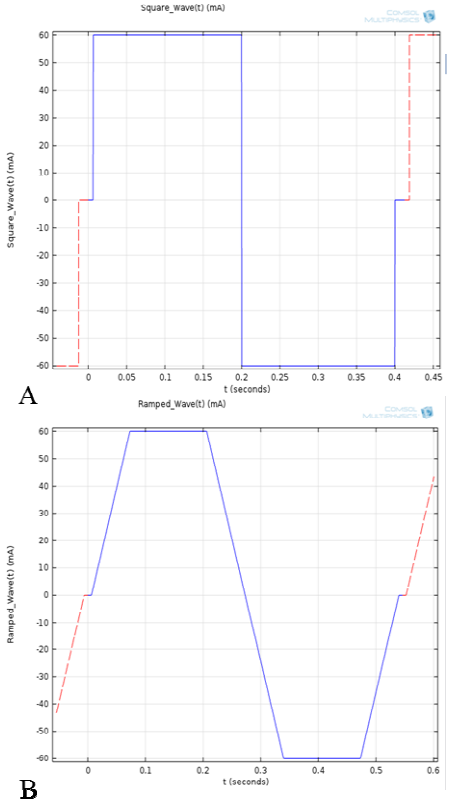

Fig. 2 These graphs show the two stimulus waveforms represented by the square wave in (A) and the edge-retarded wave in (B). In the edge-retarded wave, the ramp goes from 0 to its peak value in one RC time constant τ. The dashed lines signify that this wave is periodic

III. Results and Discussion

A. Single Pulse Analysisof Current Density

The current density and the power dissipation of a standard square wave and the edge-retarded waveform were analyzed in order to determine if a reduced amount of thermal energy enters the tissue during the edge-retarded waveform. Fig. 3 shows the current density distribution of the edge-retarded waveform compared to the square waveform. These current density distributions are normalized by a value J_o which is equal to J_{stim}in (12). This figure and all figures that follow are also non-dimensionalized along the radial axis by the radius of the electrode a. The current distributions shown in Fig. 3 represent the response to a single pulse. The current density near the edge is about 160% higher in the square wave relative to the edge-retarded waveform at its peak current density. As this behavior continues for every pulse during the duration of stimulation, the tissue near the edge of the electrode should experience more damage with a square wave than with the edge-retarded wave.

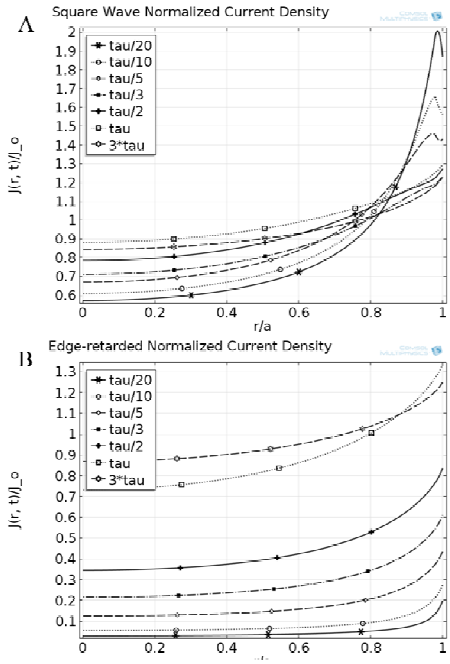

Fig. 3 Thisdepicts the current density distributions given off by the electrode with a square wave pulse (A) and an edge-retarded pulse (B). The graphs just show the electrode behavior for one pulse and this phenomenon would be repeated subsequent stimulus pulse

B. Single Pulse Analysis of Total Power Dissipation

It is also beneficial to consider the total power dissipation from the electrode for each pulse to compare the individual waveforms. In (14) and (15) the power dissipation is linked to the heating of the tissue. Fig. 4 shows the average power dissipated from the electrode surface through one complete biphasic pulse of each respective waveform. As seen on Fig. 4A, there lies a spike in the power dissipation in the middle of the pulse. This spike is due to the quick transition between the anode and the cathode of the square wave during stimulation. These quick transitions cause the current density to intensify at the edges of the electrode. With a larger current density on the electrode, (15) shows how this will cause a greater average power dissipation.When the current redistributes, the power settles back down to its average level at about $1.3x10^5$ W/m^3. The power spike reaches levels 160% greater than the peak value reached in the edge-retarded stimulation. In order to compare these two waveforms more quantitatively, the total average of the graph was calculated and plotted as a flat line across the graph. This line represents the average power dissipation per pulse. As Fig. 4 show, the total average power dissipation per pulse of the square wave is approximately $.4x10^5$ W/m^3 greater than that of the edge-retarded wave. This difference occurs even though there is the same amount of charge injection occurring in both models. The power spikes caused by the square wave and this difference in average power dissipation per pulse will compound and reveal a much more noticeable difference in tissue damage when thousands of pulses are sent into the tissue.

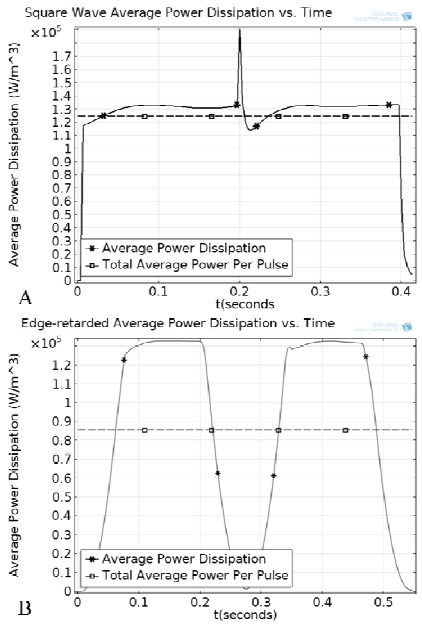

Fig. 4These plots depict the average power dissipation of the electrode in one biphasic pulse for a square wave (A) and the edge-retarded wave (B). The units of the power dissipation are W/m^3. The running average of the total pulse is shown in each graph with a flat dashed line in order to see the equivalent power dissipated per pulse. The square wave has alarger total average than the edge-retarded wave

C. Full Simulation Analysis

The main topic of interest in this study is not the current density or the power dissipation, but rather the temperature and fraction of tissue necrosis. The current density and power dissipation analysis were only signs pointing to trends that may emerge in the quantification of tissue damage. These are the main results that other electrode models have neglected to show [13]. In order to compare the edge-retarded stimulation and the square wave stimulation, the models had to compute for different time scales to provide similar charge injections. Fig. 2 shows how the edge-retarded pulses were adjusted to be longer so that one pulse injected the same amount of charge as one square wave pulse. The edge-retarded model computed a model that was three minutes long while the square wave model computed a model that was two minutes and fifteen seconds. This difference in computation times is to ensure the fact that the charge injection was similar for both computations. Using these simulation times, Fig. 5 shows the large difference in tissue temperature. The square wave reaches temperatures of 318K which is equal to 45^{o}C. In comparing these temperatures with those found in Fig. 5B from the edge-retarded stimulation, the experimental stimulation method proved to be far superior to the standard. Tissue temperatures reach above the natural skin temperature of 37^{o}C or 307.15K but they never go above standard body temperature. This demonstrates a very unique quality of the bioheat transfer equation. The ω_b term in (14) represents the blood perfusion rate of tissue. In biological mediums, the blood serves as a natural heat sink that siphons off heat from a source. The blood does have a limited capacity of heat that it can siphon off efficiency though. The heat sink capabilities of the blood compete against the heat source capabilities of the electrode and in Figs. 5A and B it is clear to see which was strongest in each case. With the square wave, the power dissipation proved to be too strong of a heat source for the blood to regulate and the tissue temperature rose. In the edge-retarded stimulation, the blood was capable of out-competing the electrode heat source and kept the body at normal bodily temperatures.

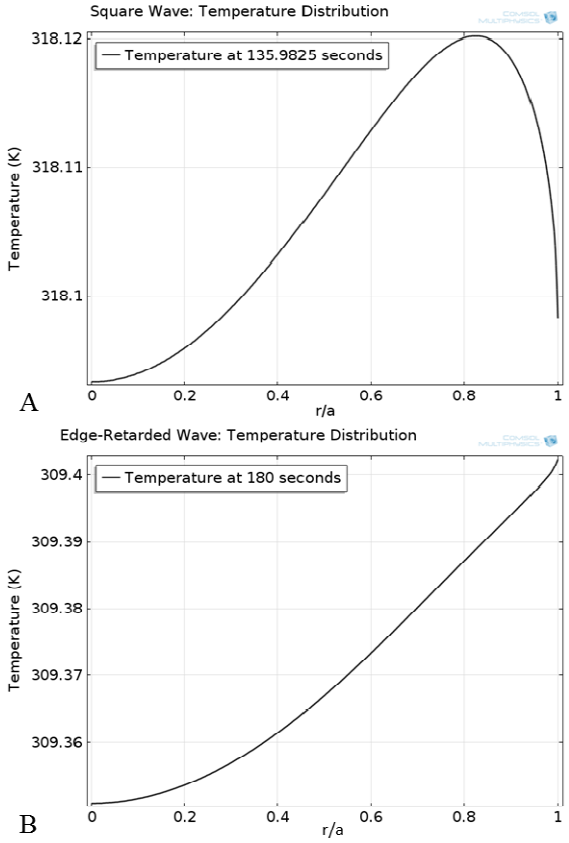

Fig. 5 This is a representation of the temperature distribution just at the electrode-tissue interface. The temperature distribution of the square wave stimulation (A) is also clearly much greater than that of the edge-retarded stimulation. For reference the magnitude of skin temperature is 307.15 K and body temperature is naturally 310/15 K

The analysis of tissue temperature distributions proved to be useful inrevealing some of the components controlling bioheat transfer. Tissue necrosis shed much light on this issue as well. Fig. 6 represents the fraction of tissue necrosis above the electrode calculated from (18). These results show that the fraction of tissue damage caused by the square wave stimulation was three orders of magnitude greater than that of the edge-retarded stimulation. The order of magnitude analysis clearly shows the value of using safer stimulation than what has been the standard.

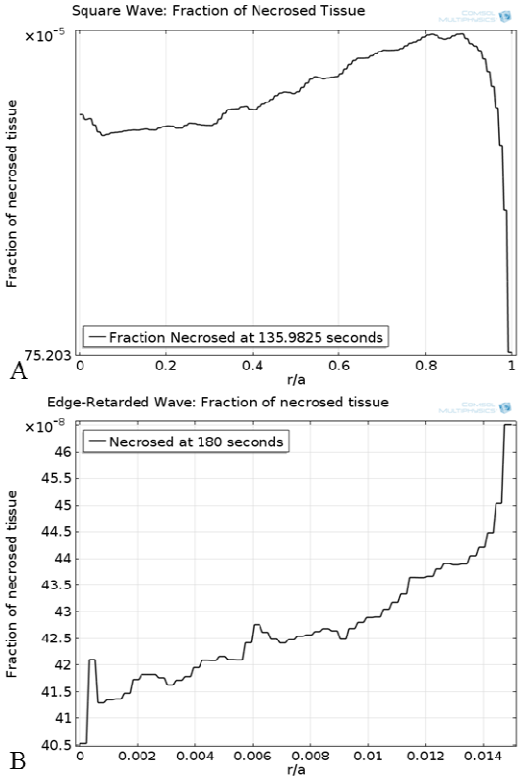

Fig. 6 Thisdepicts the fraction of tissue necrosis above the electrode. It is evident that the fraction of tissue necrosis from the square wave (A) stimulation is three orders of magnitude greater than that of the edge-retarded stimulation (B)

IV. Conclusion

This model was one of the first demonstrations of the relationship between transcutaneous stimulation and heat transfer into tissues. To model this phenomenon, this study compared normal square wave stimulation and edge-retarded stimulation to biological consequences of standard and safe stimulation [13]. The final results of the simulation revealed that square wave stimulation causes a much greater rise in tissue temperature and a much larger fraction of tissue necrosis than edge-retarded stimulation. The underlying causes of these were explainedthrough the analysis the individual pulses. The square wave involved a larger max current density, higher max power dissipation and higher average power dissipation than the edge-retarded wave. These trends are caused by the sudden changes between anode and cathode in square wave stimulation. It can be reasoned that the current density profiles and power dissipation waveforms are trustworthy signs of the level of biological changes in temperature and tissue damage found in the final results. In further research of realistic models with different parameters, this pulse data analysis can be used to predict future biological damage. The use of disk electrodes for transcutaneous stimulation of the nervous system is a common practice that will soon be adapted into other forms of research. This model also showed the value of finding safer stimulation methods. For example, the edge-retarded stimulation waveform may be

a form of stimulation which can be adapted to help make Brief Intense TENS and TSCS a more tolerable therapy for patients. On the other hand, exploring different electrode geometries can also help lower the risk of tissue damage [7]. Future work will be dedicated to studying these topics.

REFERENCES

[1] T. Watson, *Electrotherapy: evidence-based practice*. 12th ed., Edinburgh: Churchill Livingstone, 2008.
[2] D. M.Walsh,*TENS: clinical applications and related theory*. Churchill Livingstone. 1997.
[3] I. Jones, &M. I. Johnson, Transcutaneous electrical nerve stimulation.*Continuing Education in Anaesthesia, Critical Care & Pain*, vol. 9, no. 4, pp. 130-135, June 2009.
[4] S. M. Danner, U. S. Hofstoetter, J. Ladenbauer, F. Rattay, K. Minassian. Can the human lumbar posterior columns be stimulated by transcutaneous spinal cord stimulation? A modeling study. *Artificial organs*, vol. *35*, no. 3, pp. 257-262. 2011.
[5] A. J. Fong, R. R. Roy, R. M. Ichiyama, I. Lavrov, G. Courtine, Y. Gerasimenko,V. R. Edgerton. Recovery of control of posture and locomotion after a spinal cord injury: solutions staring us in the face. *Progress in brain research*,vol.175, pp. 393-418. 2009.
[6] J. D. Wiley and J. G. Webster, "Analysis and control of the current distribution under circular dispersive electrodes," IEEE Trans. Biomed.Eng., vol. BME-29, pp. 381–389, 1982.
[7] J. T. Rubinstein, F. A. Spelman, M. Soma, and M. F. Suesserman, "Current density profiles of surface mounted and recessed electrodes for neural prostheses," IEEE Trans. Biomed. Eng., vol. 34, pp. 864–875,1987.
[8] J. Newman, "Resistance for flow of current to a disk", J. Electrochem. Soc., vol. 113, 1966, pp. 501–2.
[9] J. Newman. "Frequency Dispersion in Capacity Measurements at a Disk Electrode", J. Electrochem. Soc., vol. 117, 1970, pp. 198
[10] J. Newman. "The Transient Response of a Disk Electrode", J.Electrochem., Soc., vol. 120, 1973, pp. 1339
[11] K. B. Oldham, "The RC time constant at a disk electrode,"Electrochem. Commun., vol. 6, 2004, pp. 210–214.
[12] J. C. Myland and K. B. Oldham, "How does the double layer at a disk electrode charge?", J. Electroanalyt. Chem., vol. 575, 2005, pp. 81–93.
[13] B. Wang and J. D. Weiland, "Reduction of current density at disk electrode periphery by shaping current pulse edges," in Proc. 34th Annu. Int. Conf.IEEE Eng. Med. Biol. Soc., pp. 5138–5141. 2012.
[14] M. R. Behrend , A. K. Ahuja and J. D. Weiland"Dynamic current density of the disk electrode double-layer",*IEEE Trans. Biomed. Eng.*,vol. 55,no. 3,pp.1056 -1062, 2008
[15] A. Datta, M. Elwassif, M.Bikson. Bio-heat transfer model oftranscranial DC stimulation: comparison of conventional pad versus ring electrode. *31st Annual International Conference of the IEEE Engineering in Medicine and Biology Society. IEEE Engineering in Medicine and Biology Society. Conference.* 670-673, 2009.
[16] J. T. Rubinstein , F. A. Spelman , M. Soma and M. F. Suesserman"Current density profiles of surface mounted and recessed electrodes for neural prostheses",*IEEE Trans. Biomed. Eng.*,vol. BME-34,no. 11,pp.864 -875 1987
[17] A. Zolfaghari, M. Maerefat, "A new simplified thermoregulatory bioheat model for evaluating thermal response of the human body to transient environments." Build Environ, vol. 45, no. 10, pp. 2068–2076, 2010.
[18] C.Gabriel, S. Gabriel, E.Corthout, "The dielectric properties of biological tissues: I. Literature survey," Phys. Med. Biol. Vol. 41, pp. 2231-2249. 1996.
[19] S.Gabriel, R.W. Lau, C. Gabriel, "The dielectric properties of biological tissues: II. Measurements in the frequency range 10 Hz to 20 GHz," Phys. Med. Biol. Vol. 41, pp. 2251-2269. 1996
[20] S.Gabriel, R.W. Lau, C.Gabriel, "The dielectric properties of biological tissues: III. Parametric models for the dielectric spectrum of tissues," Phys. Med. Biol. Vol. 41, pp. 2271-2293. 1996
[21] K. R. Diller, J. A. Pearce,"Issues in modeling thermal alterations in tissues," NY Acad. Sci. vol. 888, pp. 153–164, 1999
[22] N.T. Wright, "On a relationship between the Arrhenius parametersfrom thermal damage studies," J. Biomech. Eng. Vol. 125, pp. 300–304, 2003